

Investigation of the Multiaxial Constitutive Behavior of PLZT under Electrical Cycling

R.C. Rogan,¹ E. Üstüncü,¹ M.R. Daymond,² U. Lienert,³ J. Almer,³ D. Haefner³

¹California Institute of Technology, Pasadena, CA, U.S.A.

²Rutherford Appleton Laboratory, Chilton, Didcot, Oxon, United Kingdom

³Advanced Photon Source (APS), Argonne National Laboratory, Argonne, IL, U.S.A.

Introduction

Piezoelectric materials exhibit a coupling between the applied stress and electric field. This property makes them useful materials for both sensors and micromechanical actuators. Some of the most commercially successful piezoelectric compositions come from the series $\text{Pb}(\text{Zr}_x\text{Ti}_{1-x})\text{O}_3$ (PZT). Substituting La for Pb yields transparent materials (PLZT) that have tunable electro-optical properties, making them suitable for several optical applications. Recently, there has been much debate over the mechanism of ferroelectric-ferroelastic coupling in relaxor ferroelectrics such as PLZT. At the optimally doped composition (8% La substitution), transmission electron microscopy (TEM) observations indicate that long-range ferroelectric order is replaced by short-range order in the form of nanopolar domains [1-6]. In an effort to better understand the multiaxial nature of the ferroelectric constitutive behavior of PLZT, 2-D transmission x-ray diffraction experiments were conducted on specimens under electrical loading at beamline station 1-ID-C at the APS.

Methods and Materials

$(\text{Pb}_{0.92}\text{La}_{0.08})(\text{Zr}_{0.65}\text{Ti}_{0.35})\text{O}_3$ ceramic specimens were examined by using an area detector in transmission geometry that employed an 80-keV, $100 \times 100\text{-}\mu\text{m}^2$ beam. Experimental geometry was calibrated by using a cerium oxide standard to ensure accurate lattice parameter measurements. The PLZT specimen measured 2.2-mm wide, 8-mm long, and ~ 0.9 -mm thick. Silver electrodes were painted to the sides of the sample in order to apply electric fields across the 2.2-mm width. The sample was aligned such that the x-ray transmission occurred normal to the 0.9-mm sample thickness and the electric field would be parallel with the $\eta = 0^\circ$ direction of the Debye rings (Fig. 1). After initial characterization, static electric fields were applied to the specimen in steps of 0.09 kV/mm. After each voltage change, diffraction patterns were recorded. First the sample was “poled” from the random, sintered configuration by applying fields up to -0.9 kV/mm. (Poling requires fields beyond the coercive field E_c of the material to align domain polarizations.) Then the sample was subjected to a complete electrical loading cycle, ranging from 0.9 to

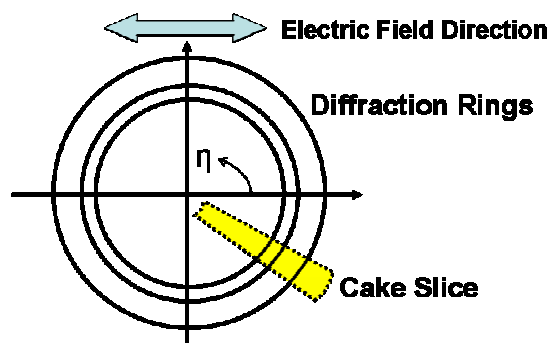


FIG. 1. Schematic of experimental geometry and data partitioning for analysis.

-0.9 kV/mm. Finally, it was relaxed back to the zero field condition. Diffraction patterns were divided into 10° azimuthal “cake slices” in η , each yielding a full diffraction pattern representative of PLZT’s response to the electric field applied at a specified angle.

Initial attempts to fit the data by using whole pattern Rietveld [7] analysis met with limited success. Historically, PLZT compositions have been assigned a myriad of crystal structures depending on slight compositional differences and preparation conditions. While the parent phase of our PLZT material [undoped $\text{Pb}(\text{Zr}_{0.65}\text{Ti}_{0.35})\text{O}_3$] has a clear rhombohedral crystal structure, La doping has recently been shown to destroy long-range crystal symmetry by forming polar nanodomains with varying degrees of oxygen octahedral tilt [2]. In contrast to typical ferroelectric materials, which possess large (micrometer) regions of aligned polarizations, the octahedral tilt disorder in PLZT leads to nanodomain formation and the disruption of long-range internal electric fields. Recently, theoretical models describing PLZT-type ferroelectric materials as dipolar glasses with random internal electric fields have met with success [8-10].

Results

The effects of nanodomains on diffraction data became evident when we attempted to assign a crystal structure to

PLZT. While the peak locations indicate a cubiclike structure, Rietveld analysis using a generic cubic perovskite produced inappropriate peak intensities. Attempts to fit the data by using rhombohedral and orthorhombic settings as well as all combinations of these space groups did not improve fits with respect to the cubic approximation. Despite the inability of these structures to accurately model all information contained in the diffraction patterns, the cubic structure description gave sound results for all peak positions. As such, we decided it is an appropriate model to analyze lattice strains in this system.

Figure 2 displays the results of the cubic strains resulting from the initial poling process as a function of η . As the field is raised, there is no significant strain induced in the system until the coercive field is reached at ~ 0.33 kV/mm. At this point, the curves for each η diverge significantly, leading to tensile strain along the field and compressive strain perpendicular to it. This is consistent with the interpretation that the electric field causes domain switching, so that dipoles within domains align with the field, and the field, once aligned interacts with the dipoles to increase the lattice strain parallel to it. The compressive strains observed in perpendicular directions are nothing more than the associated Poisson effect.

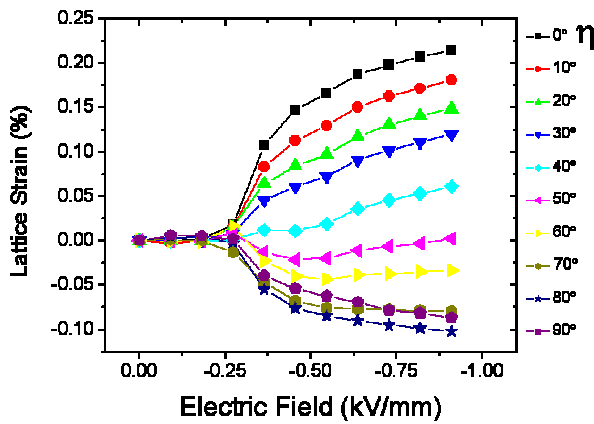


FIG. 2. Strains measured during the poling process as a function of angle with respect to the electric field.

These data may be presented in a more intuitive fashion by plotting the poling span, or the final strain induced by poling, as a function of η in a polar plot (Fig. 3). Note here that the maximum strain values occur along the direction of the electric field and that all results appear symmetric about the field direction. Zero strain values occur at approximately 50° to 55° from the field direction. The crystallographically limited ferroelectric switching mechanism of typical (undoped) rhombohedral PZT

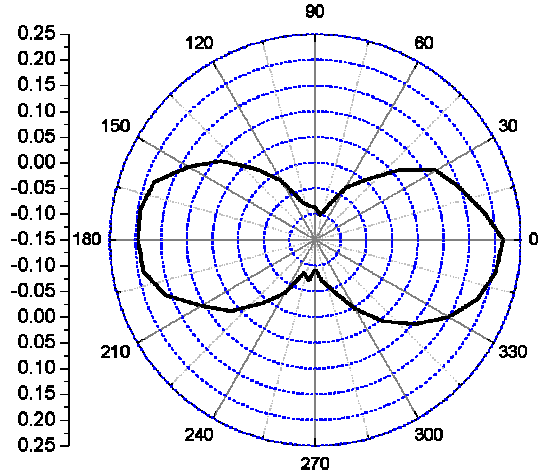


FIG. 3. Poling spans as a function of angle. The radial axis is in units of strain %.

induces large strains in the direction of crystal polarizations (71° and 109° in this geometry) during electromechanical cycling. The lack of any significant features in the presented strain data for PLZT near 71° and 109° from the poling field suggests that this mechanism is not active at significant length scales in this composition. Figure 3 emphasizes the power of using a 2-D transmission geometry: a complete multiaxial data set can be simultaneously measured from one specimen, avoiding the need for laborious sample sectioning, repetitive testing, and sample-to-sample errors.

After material poling was completed, the electric field was cycled in order to produce the “butterfly” curves shown in Fig. 4. Note that the coercive fields (as measured from the bottom tips of the “wings”) indicated during the cycling procedure are again $\sim \pm 0.33$ kV/mm. Even after forcing large strains into the crystal by aligning a significant portion of the crystal dipoles, we still observe the same coercive field to initiate domain switching in either field direction. However, as the coercive field is reached, poling strains are not completely relaxed to zero before ferroelectric switching is once again activated and strains begin increasing. The effect of poling strains is finally seen in the large residual strains present in the PLZT sample after relaxation back to zero field (Fig. 5).

Discussion

The data presented here support the concept of PLZT ferroelectrics modeled by using “glasslike” phenomena [1-6]. In this case, typical ferroelectric crystal structures are not observed at any point in the electrical loading. In our work, by approximating the structure as cubic, significant strain information could be obtained. Strain

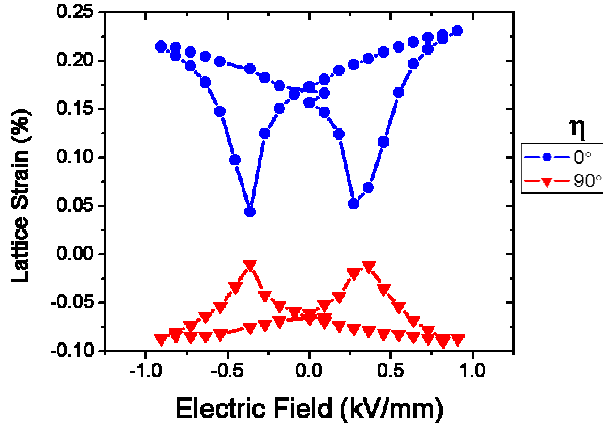


FIG. 4. “Butterfly” loops resulting from electrical cycling. Curves begin near -1.0 kV/mm, progress to 1.0 kV/mm, and return to -1.0 kV/mm.

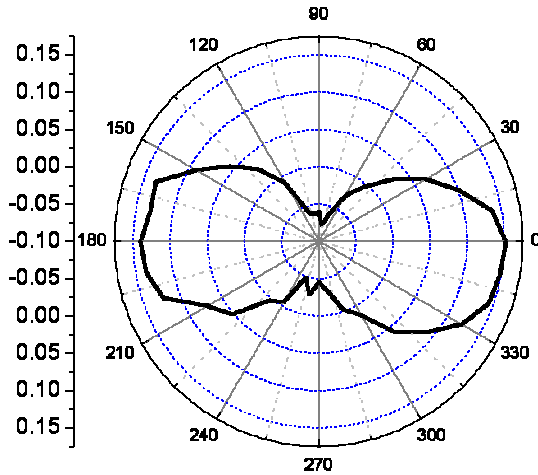


FIG. 5. Residual strains after cyclic loading as a function of angle with respect to the poling field.

results indicate a lack of typical ferroelectric switching behavior restricted by crystal symmetry; instead the appearance is akin to a “glasslike” material in which no preferred orientations are favored. Still, the presence of residual strains after electric cycling implies the presence

of crystal stresses locked in by the reorientation of unit cell dipoles. The power of a multiaxial diffraction experiment is essential in completely understanding the constitutive behavior of ferroelectrics, since information about all angles with respect to applied forces is needed to ascertain material characteristics. We are currently adapting a self-consistent model [11] to compare to our diffraction data [12] and deduce material properties.

Acknowledgments

This work is funded by the National Science Foundation (CAREER Grant No. DMR-9985264) and the Army Research Office (Grant No. DAAD19-01-1-0517). The APS is supported by the U.S. Department of Energy, Office of Science, Office of Basic Energy Sciences, under Contract No. W-31-109-ENG-38.

References

- [1] J.F. Li, X.H. Dai, A. Chow, and D. Viehland, *J. Mater. Res.* **10**(4), 926-938 (1995).
- [2] X.H. Dai, Z.K. Xu, and D. Viehland, *J. Am. Ceram. Soc.* **78**(10), 2815-2827 (1998).
- [3] X.H. Dai, Z. Xu, and D. Viehland, *Philos. Mag.* **70**(1), 33-48 (1994).
- [4] X.H. Dai, Z. Xu, J.F. Li, and D. Viehland, *J. Mater. Res.* **11**(3), 618-625 (1996).
- [5] Z. Xu, M.C. Kim, J.F. Li, and D. Viehland, *Philos. Mag. A* **74**(2), 395-406 (1996).
- [6] C.A. Randall, D.J. Barber, and R.W. Whatmore, *J. Microscopy-Oxford* **145**, 275-291 (1987).
- [7] H.M. Rietveld, *J. Appl. Crystallog.* **2**, 65 (1969).
- [8] V. Bobnar, Z. Kutnjak, R. Pirc, R. Blinc, and A. Levstik, *Phys. Rev. Lett.* **84**(25), 5892-5895 (2000).
- [9] M. El Marssi, R. Farhi, J.L. Dellis, M.D. Glinchuk, L. Seguin, and D. Viehland, *J. Appl. Phys.* **83**(10), 5371-5380 (1990).
- [10] D. Viehland, and Y.H. Chen, *J. Appl. Phys.* **88**(11), 6696-6707 (2000).
- [11] J.E. Huber, N.A. Fleck, C.M. Landis, and R.M. McMeeking, *J. Mech. Phys. Solids* **47**(8), 1663-1697 (1999).
- [12] R.C. Rogan, E. Ustundag, U. Lienert, and M.R. Daymond, *J. Appl. Phys.* (to be submitted, 2003).